Multiple Multipole Method Applied to an Exposure Safety Study

Niels Kuster[1]
Swiss Federal Institute of Technology

Abstract - A summary of the three-dimensional implementation of the multiple multipole method (3D MMP) is given, followed by discussions on the method's advantages and limitations on the basis of an example study. The advantages are seen in its quantitative validation capability, in its efficiency for smoothly shaped bodies and its achievable accuracy, in particular, near surfaces. However, MMP's greatest strength appears to be with problems with EM sources in the closest vicinity of lossy bodies. This is shown by a condensed presentation of a study investigating the RF exposure safety of UHF and VHF transmitters commonly used by radio and TV crews for onsite live reports. In addition to gaining knowledge about the local SAR distribution, the goal of this study was to assess necessary safety distances for given threshold values. The presented study was performed with the 3D MMP software package on a 80386 based PC laptop extended by a 80860 board with 32 MB RAM.

1 Introduction

In the 1970's and early 1980's, various analytical and numerical approaches were suggested and applied to study the absorption of biological bodies under far field exposures. Far field conditions were studied because of their relevance to setting exposure safety guidelines. The other reason is that the computers and numerical techniques available at that time were hardly suited for near field computations. Exposures to strong far fields are rare, even within occupational groups (i.e., radar workers), while extensive near field exposures are much more frequent (i.e., welders, antenna service workers, etc.). With the recent growth in popularity of mobile communications, more and more of the general population is exposed daily to small transmitters operating in the closest vicinity of the user's head.

Early attempts to study these dosimetric problems were of limited success because of shortcomings in the methodology of the applied numerical techniques, such as IEBCM [Iskander et. al., 1987] and MoM [Stuckly et. al., 1986] for near field exposures. More appropriate are two methods developed and utilized for such applications within the last few year, namely, FDTD [Chen and Gandhi, 1989] and 3D MMP [Kuster and Ballisti, 1989; Kuster and Balzano, 1992]. The latter is the subject of this paper. A comprehensive summary of MMP is given followed by a discussion on the basis of a dosimetric assessment study. More detailed overviews on methodology, code and simulation technique are described in [Hafner, 1990], [Bomholt, 1990], [Kuster, 1993].

2 MMP Method

The most fundamental ideas of MMP were first proposed by Hafner [Hafner, 1980]. However, similar techniques have been developed independently around the world during the last decade. [Ludwig, 1989] summarizes these techniques and adopts the name generalized multipole technique (GMT).

[1]Author address: Swiss Federal Institute of Technology (ETH), CH-8092 Zurich, Switzerland

2.1 Basics of GMT

Generalized multipole technique is the generic term for methods approximating the unknown (scattered) field F in each domain by several (P) sets of functions F_i with different origins located inside or outside the domain but not on the boundaries. Each set consists of a limited number N_i of basis functions f_{ij}, which are analytical solutions of Maxwell's equations for linear and homogeneous materials.

$$F = \sum_{i=1}^{P} F_i = \sum_{i=1}^{P} \sum_{j=1}^{N_i} c_{ij} f_{ij} \tag{1}$$

As the name GMT implies, the primary expansion functions are finite series of multipole solutions of the Helmholtz equations (in the following simply referred to as multipoles). The unknown parameters c_{ij} are numerically evaluated by enforcing the boundary conditions on a discrete set of points on the boundary.

Hence, the methods based on GMT are applicable to static or time-harmonic electromagnetic boundary value and eigenvalue problems within piecewise linear and homogeneous domains. The different methods distinguish themselves in the sets of basis functions used and the matching technique applied. Most use several multipoles with different origins for the same boundary adapted to its geometry in order to increase the flexibility and convergence properties of the technique. This approach was not considered initially because of a dependence between analytical, infinite expansions in the same locations. However, finite multipole functions have a very local behavior which can be exploited to achieve sufficient independence between different multipoles. This idea is analogous to the charge simulation method for electrostatics and is further illustrated by the Huyghens principle.

In the following, only the sets of basis functions and the matching technique implemented in the 3D MMP software package are discussed.

2.2 Basis Functions

The most flexible set of basis functions implemented in the 3D MMP software package are *multipoles*, which are obtained from the Helmholtz equation by separation of variables in spherical coordinates

$$\tilde{f}_{ij} = h_n^{(1)}(kr_i) P_n^m(\cos\vartheta_i) \begin{matrix}\cos\\ \sin\end{matrix}(m\varphi_i) \tag{2}$$

where the $h_n^{(1)}$ are spherical Hankel functions of the first kind ($e^{-i\omega t}$ time dependence) and P_n^m are associated Legendre functions. The vectorial f_{ij} are deduced by simple derivations from the scalar $\tilde{f}_{ij}$ [Bomholt, 1990]. The functions f_{ij} are singular in their origins ($r_i = 0$) and must be placed outside the domain in which the field is expanded. The use of several multipoles of different orders along the same boundary led to the method's name "multiple multipole". Simple geometrical rules have been developed to obtain a sufficient base and while avoiding numerical dependence.

Multipoles are most efficient if a large area of the boundary can be covered by one multipole. For long and thin structures, a large number of multipoles must be set up because the largest possible distance to the boundary is small compared to the length of the structure.

This approach is especially poor for thin wire structures, which are also often involved in bioelectromagnetic applications (e.g., sources such as antennas or implants such as a pace maker). To avoid this rather significant shortcoming, *line multipoles* are implemented [Leuchtmann, 1991]. The electrical zero order term corresponds to the *thin wire approximation* with the segment currents

$$I(z') = I_a \cos kz' + I_b \sin kz' \tag{3}$$

along the z'-direction (k is the complex propagation constant of the surrounding medium). The corresponding field values can be evaluated in simple analytical terms. The fields of higher order multipoles are not axisymmetrical but vary with $\begin{matrix}\cos\\ \sin\end{matrix}(m\varphi)$. This implementation might also be seen as a combination of NEC with GMT.

In some cases, so called *normal expansions* are very convenient and efficient to use. They are formally equal to (2), but the Hankel functions are replaced by Bessel functions. There is no singularity at the origin of the normal expansions, and they usually do not have a local behavior. Inside lossy media, the values of these functions even grow with distance. Physically they describe a superposition of incoming and outgoing waves. Only one normal expansion should be used for a domain, preferably placed inside the domain. They are especially suited for spherical or rather spherical domains and are often more efficient than multipoles, especially if symmetries are exploited. Furthermore the validation of the result is simplified.

Another important function, called *connection*, is a linear combination of basis functions, where each function has a *known* parameter c_k:

$$f_i = \sum_{k=1}^{N} c_k f_k \tag{4}$$

Connections may also be nested, i.e., f_k may itself be a connection. This is a very powerful macro feature and the basis of the iterative simulation technique, which considerably extends the capability of the code. In this context, the solution of one step is packed into a connection and used as excitation for the next step, i.e., the basis functions f_{ij} become f_k and the solved parameters c_{ij} become c_k.

Other expansion functions for special purposes may be introduced without any difficulty, e.g., *plane waves*, *waveguide modes* and many others. Typically they are used as excitation.

2.3 Matching Technique and Solution of the Matrix Equation

Besides using more general basis functions, MMP distinguishes itself from the other GMT based methods through its applied matching technique. Instead of the simple point matching, a *generalized point matching* technique (GPM) with many more matching points (and equations) than necessary is used. Moreover, all 6 boundary conditions for a general surface can be enforced instead of only 4 linearly independent ones. The resulting overdetermined system of equations is solved in the least squares (LS) sense. In 2D, a 2 to 3 times overdetermined system is considered to be sufficient [Hafner, 1990], whereas in 3D, the use of 4 to 10 more equations is recommended because of the directionality of the spherical expansions [Kuster, 1993]. With the selected weighting functions – important for LS – GPM becomes numerically equivalent to an error minimization technique or a moment method with Galerkin test functions [Hafner, 1990]. As a consequence, the error is much more smoothly distributed over the surface and the solution is much less sensitive to the location of single matching points. An additional and important advantage is that the discretization is now largely independent of the choice of basis functions, which dramatically simplifies the modeling process.

The price for these advantages is an increased numerical effort because the obtained system of equations

$$A\ c = b \tag{5}$$

is strongly rectangular. Although strong dependence is avoided by using empirical rules for pole-setting, weighting, etc., the matrix A tends to be ill-conditioned for more complex problems. QR decomposition methods are therefore preferred being less sensitive to the condition number $\kappa_2(A)$

[Gentleman, 1975], [Golup and Loan, 1989] than the more efficient method of normal equation. Among the QR decomposition methods, Givens transformations is selected. Although it requires more operations than comparable algorithms (e.g., Fast Givens or Householder), it has the important advantage that the matrix A can be processed row by row, as it is formed. Therefore, only an upper triangular matrix R (Cholesky factor of A^*A) with $n(n+1)/2$ elements needs to be stored.

The matrix A has additional numerically interesting properties that depend on the problem but are worth being exploited. For most applications, A can be arranged on the basis of physical considerations such that a square block matrix with strongly diagonal dominance is obtained. This matrix is solved through a block iterative technique that is equivalent to Gauss-Seidel block iteration. This technique has important advantages regarding modeling which even surpass the important numerical benefits. A detailed discussion of this technique is given in [Kuster and Bomholt, 1993].

2.4 Symmetries

The geometry of boundary value problems is often symmetric, i.e., invariant to certain symmetry transformations in space. As a result, the boundary value problem can be split up into a number of smaller, symmetry adapted problems which can be solved separately at lesser overall expense.

$$Ac = b \qquad \rightarrow \qquad A_l c_l = b_l \qquad (l = 1, \ldots, L) \tag{6}$$

In the 3D MMP code, reflective symmetries on the orthogonal planes $X = 0$, $Y = 0$ and $Z = 0$ can be fully exploited [Bomholt, 1990], i.e., $L_{max} = 8$. Additionally, some of these symmetry parts may be left out *a priori* if the corresponding symmetry part of the excitation disappears, which further reduces expense.

Connections are fully compatible with symmetries, i.e., connections of higher symmetries may be introduced into problems with lower symmetry and connections with lower symmetry into problems with higher symmetries.

2.5 Software and Hardware

The kernel software of the 2D and 3D MMP implementations are written in a very portable FORTRAN and published in [Hafner, 1990b] and [Bomholt, 1990], respectively. These codes run on a wide range of computers such as personal computers from the XT-compatible to the 8048 powered machines, floating point boards based on the 80860 processor, workstations and different mainframes. Additionally, the code was parallelized for transputer (T800) networks or SUN networks.

A software package with which the input files for general problems can be efficiently generated and the solution can be visualized and validated is at least as important as the method and its implementation. For the 3D MMP code, two sophisticated graphic input and output interfaces have been developed for PC's and SUN workstations [Regli, 1989]. The input interface allows for easy surface discretization and helps the user in the choice of multipoles. With the output interface a large variety of plots can be drawn and animated.

All of the simulations described in the following have been performed on a 386 based laptop computer extended by an 80860 board with 32 MByte memory.

3 Example Study

The more sincere way to illustrate and discuss the applicability and limitation of a technique and its implementation is on the basis of a performed study than with any method-matched examples.

Thus, some parts of a dosimetric assessment performed for public broadcasting organizations are presented and discussed in the following. The objective of the study was to clarify the safety questions of the mobile transmitters commonly used for on-site live reports by radio and TV crews. The broadcasters specifically were interested in information regarding the actual local distributions of the specific absorption rate (SAR) and for the evaluation of safety distances, which ensure the compliance with current and proposed SAR safety limits, in particular with the newest revision of the German standard [DIN VDE 0848 Part 2, 1991]. As the discussions on the most appropriate averaging weights still continue, different averaging weights are analyzed.

3.1 Transmitters

The investigated reportage transmitters were conceived for on site reports for radio and television crews. A high quality broadband transmitter with a matched antenna is used to submit reports, while a simple narrow-band receiver using the same antenna is sufficient to receive the producer's instructions. The devices are offered in various configurations which also use different frequency bands.

UHF-Types

The newer devices transmit in the UHF range between 540 and 790 MHz. Thirty two channels are distributed upon a total bandwidth of 185 MHz, which requires a tunable antenna (cf. Figure 1). The thicker part of the antenna corresponds to a center fed $\lambda/2$ dipole (monopole with a mode suppression filter or $\lambda/4$ balun) whose length may be adjusted for the given frequency with the help of an SWR-meter. The VHF signal is received by the same antenna, which is lengthened by the capacitive-coupled extension for this purpose. The antennas can be mounted directly on the device or on a special shoulder belt (cf. Figure 1c). The latter improves the quality of the transmission. However, in this case the antenna is in the closest vicinity of the head and, therefore, to those organs which may be the most sensitive to EMF (the eyes and brain).

First the output impedance of the HF amplifier and the feedpoint antenna depending on its position to the body is measured as both determine the feedpoint current and therefore the SAR values [Kuster and Balzano, 1992]. The equivalent output impedance of the HF amplifier is about $Z = (50 - i15)\Omega$ for both power levels. The structure of the symmetrical UHF-Antenna is relatively complex and difficult to measure. Extensive measurements for various well defined positions are unnecessary because reliable worst case SAR can be assessed with a good estimate on the minimum antenna impedance. The more qualitative measurements were performed with a network analyzer HP8783A calibrated at the location of the coaxial connector of the antenna. This calibration was then corrected by the electrical length between driving point and connector, which was approximately determined in a previous measurement. Using this set-up, measurements of the feed point impedance are performed at different antenna distances from the head of a test person. The lowest feedpoint impedance measured was larger than 40 Ω. This finding indicates that the antenna current does not largely depend on the distance between antenna axis and surface of the body.

VHF-Types

Some types of the same device operates in the VHF-range between 220 and 240 MHz with no more than 16 channels of maximum 5 MHz bandwidth and a nominal power of 10 W (switchable to 5 watt). The ($\lambda/4$) monopole antenna, illustrated in Figure 1b, has a fixed length. Its impedance is matched to the respective transmitter. It can be mounted either on the device or just above the shoulder on a special belt. To obtain a better defined counterpoise for the shoulder mounted

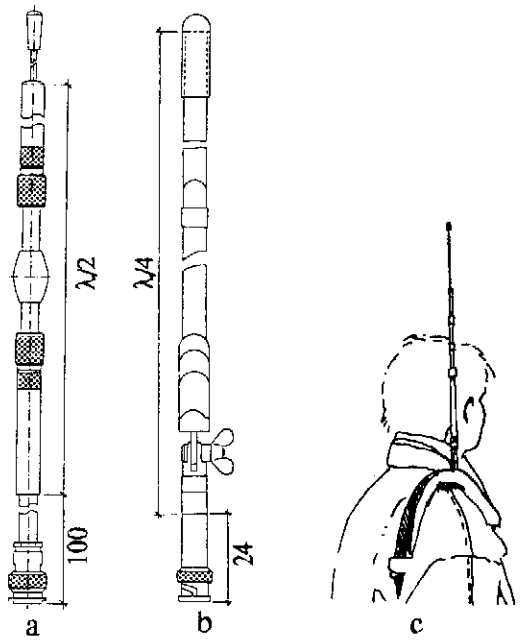

Figure 1: a) UHF dipole antenna; b) VHF monopole antenna; c) the UHF dipole and the upper band VHF monopole antennas may be worn on a special shoulder belt, as illustrated here. Measure in mm.

monopole antenna, a $\lambda/4$ choke for sheath current suppression is integrated into the cable, which feeds the antenna and is mounted on the shoulder belt. Therefore, the choke is almost attached to the surface of the body and results in a strong coupling to the body. In other words, the choke and the body of the user are an integral part of the radiation mechanism, providing the return current to the $\lambda/4$ monopole. This fact must be discussed in greater detail below.

Many different types of the former device family have been produced, which operate between 70 and 230 MHz. Generally, they all have a nominal power of 10 W which can be switched down to 1 W. The antenna is also a monopole antenna with constant length, which is mounted only on the device (cf. Figure 1b).

3.2 Numerical Models

Obviously, a detailed modeling of the human body with its immense complexity is far beyond any scope. In addition, the variations between people are significant on a coarse scale. Detailed simulations of the transmitters that cover all important parameters regarding the absorption are also not without any problems. Therefore, and particular with in respect to safety questions, the simulation of "worst case" situations is the primary goal. The basic idea behind safety standards is to define the limits by factors below the known threshold values (safety factor). Therefore, artificial "worst case" situations are not considered in the following. Instead realistic, extreme situations, which might occur in practice over a longer time period ($>$ 6 min.) are studied.

The following numerical models are as simple as the "worst case" assessment allows. It is known from the interaction mechanism in the near field of dipole antenna [Kuster and Balzano, 1992] that the most important parameters are the frequency and feedpoint current and the distance of the antenna from the tissue. The inhomogeneties of the body are less important than previously anticipated.

Transmitters

The transmitting part of the UHF antenna is a symmetrical, centrally fed antenna with a well defined driving point impedance. A well suited model for this type of antenna is a thick dipole with the appropriate dimensions.

Not as well defined is the impedance of the monopole type of antenna for the VHF device, because the electrical counterpoise consists of either the enclosure of the device or the $\lambda/4$ choke together with the body of the user. A detailed numerical simulation of the transmitter would go beyond the scope of this project. The transmitting antenna was easily simulated with an asymmetric dipole with maximum current at the feeding point. Possible deviations in the absorption rate caused by these simplifications will be discussed and estimated at the end of this paper.

Using line multipoles, the modeling of the transceivers essentially corresponds to that of codes based on the thin wire approximation, i.e., NEC. More accurate models would be possible, but are not required for this assessment.

Human Model

The previously used models of the human body [Hafner and Kuster, 1991] are improved in order to obtain more realistic geometrical conditions for the simulation of the device-mounted or body-mounted antennas. The model is illustrated in Figure 2 and its simulation is described in detail in [Kuster, 1993]. Although the model is divided into several layers for computational reasons, it is homogeneously characterized using the electrical parameters of human muscle tissue. This is necessary as muscle tissue is the most highly conductive tissue and therefore most appropriate for assessing worst case SAR values. The parameters used for the head correspond to either brain-like or muscle-like tissues. Such significant simplifications of the human body are permitted because the body's inhomogeneities do not significantly modify absorption in this frequency range [Kuster and Balzano, 1992] . In order to underscore this argument, two further simulations are performed using the same human shape but additionally modeling either the skull or the kidneys (Figure 3). The values for the electrical parameters are obtained by interpolating the values given by [Pethig, 1984]. The mass density is in the following discussion assumed as 1 g/cm^3 for reason of simplicity.

3.3 Validation of the Solutions

Special care must be taken regarding the validation of the solutions because the quality of the assessment entirely depends on the quantitative accuracy. Two checks are performed.

First, the results are validated by applying the procedure for solution validation [Kuster, 1993], which was developed for MMP and the tools of which are integrated into the 3D MMP software package. These internal check routines have proven to be highly reliable, at least for simply shaped bodies, such that experimental control measurements can be avoided for many applications.

Second, the physical plausibility of all solutions are checked with the energy absorption mechanism extracted on the basis of experimental measurements and numerical computations [Kuster and Balzano, 1992]. The spatial local peak SAR values are compared with those obtained with the approximation formula derived in the same paper.

3.4 Results

The results of the simulations are illustrated in the following Figures 4 - 10 and summarized in Tables 1 - 4. It is important to note that all values are normalized to a feeding point current of 141 mA (1 W on 50 Ω) and 447 mA (10 W on 50 Ω), respectively. The figures show the SAR

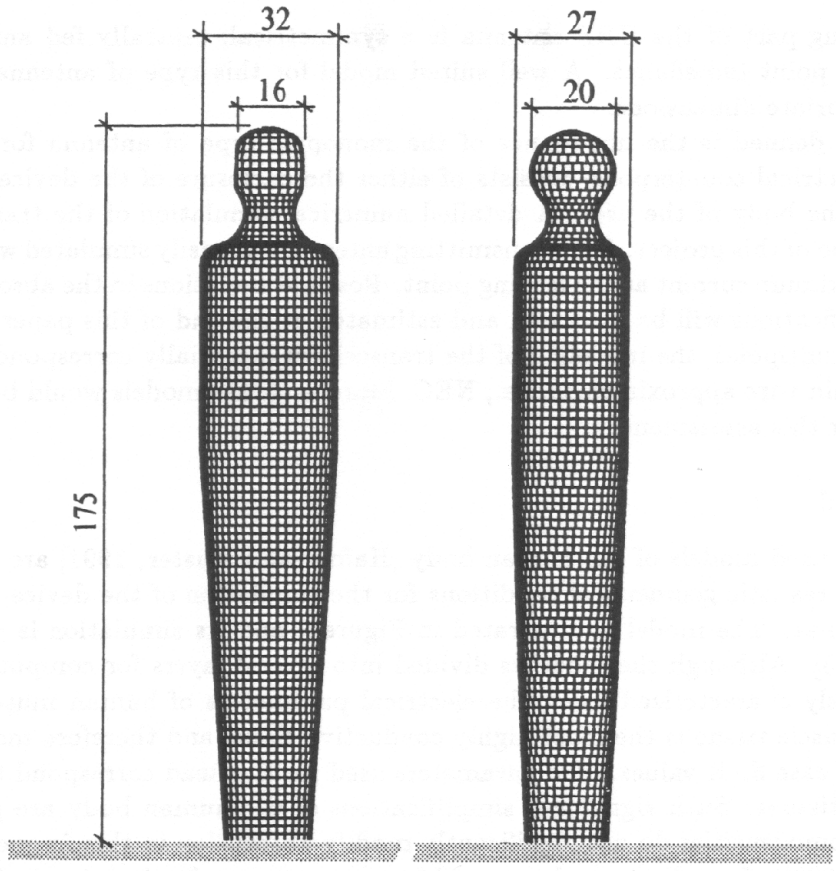

Figure 2: Longitudinal and cross section of the human model used (measured in cm).

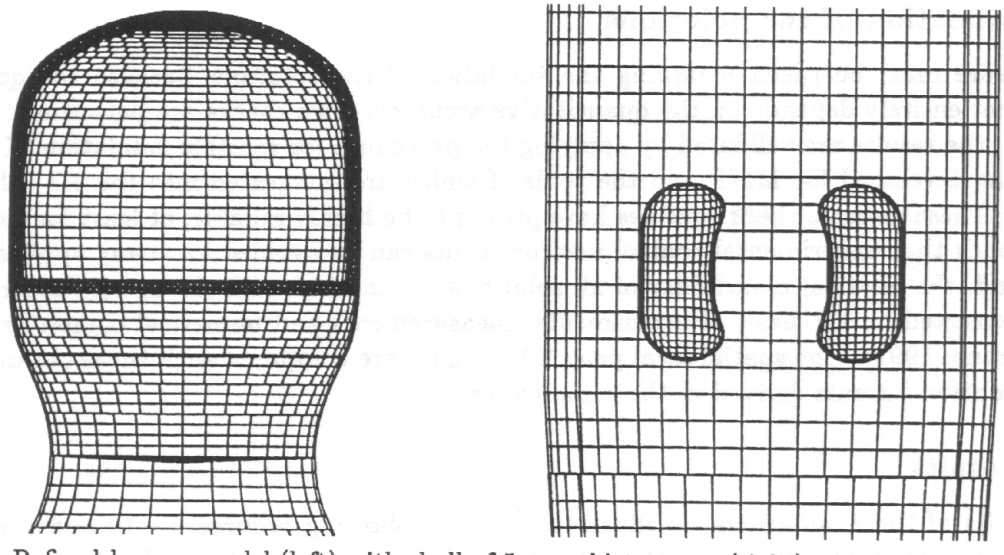

Figure 3: Refined human model (left) with skull of 5 mm thickness or (right) with kidneys (h = 10 cm).

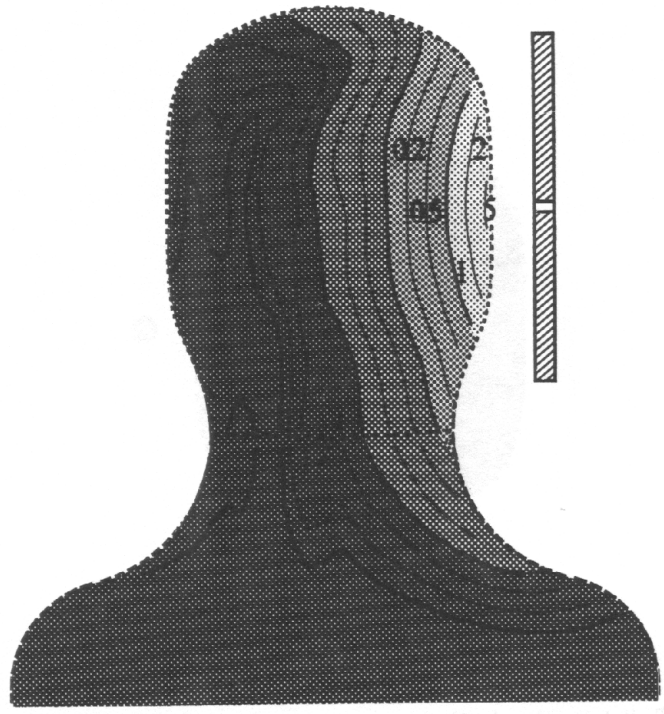

Figure 4: SAR [mW/cm^3] distribution in the longitudinal section. Simulation of the body mounted UHF antenna (f = 750 MHz) at the distance of 2.5 cm from the surface of the head. The parameters of the simulation are: I_{fp} = 141 mA; head and body: ε_r = 55, σ = 1.4 mho/m (which correspond to muscle tissue).

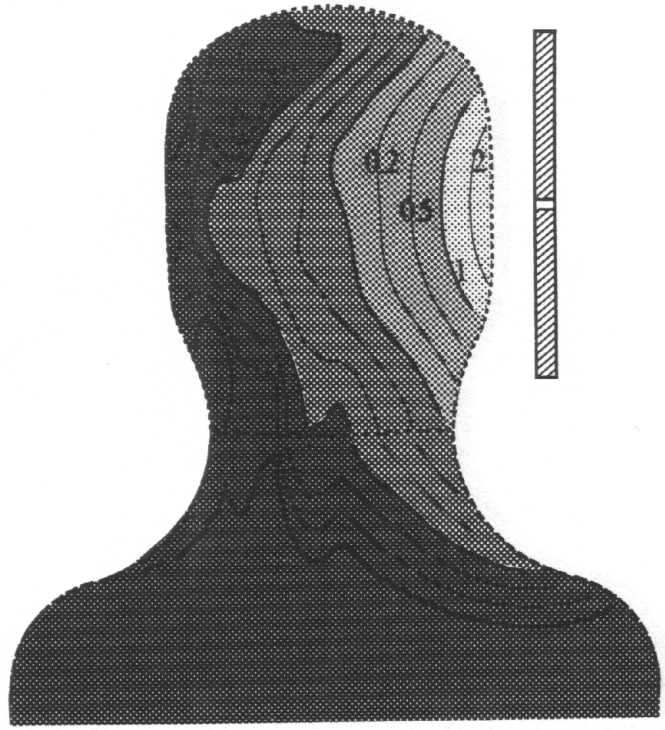

Figure 5: SAR [mW/cm^3] distribution in the longitudinal section. Simulation of the body mounted UHF antenna (f = 750 MHz) at the distance of 2.5 cm from the surface of the head. The parameters of the simulation are: I_{fp} = 141 mA; head: ε_r = 45, σ = 0.75 mho/m (which correspond to brain tissue); body: ε_r = 55, σ = 1.4 mho/m (muscle tissue).

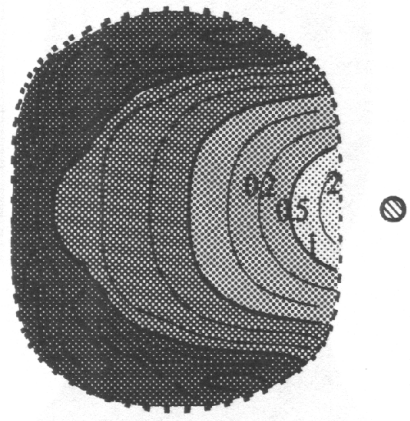

Figure 6: SAR [mW/cm^3] distribution in the cross section at the level of the antenna feedpoint. Simulation of the body mounted UHF antenna (f = 750 MHz) at a distance of 2.5 cm from the surface of the head. The parameters of the simulation are: $I_{fp} = 141$ mA; head: $\varepsilon_r = 45$, $\sigma = 0.75$ mho/m (brain tissue); body: $\varepsilon_r = 55$, $\sigma = 1.4$ mho/m (muscle tissue).

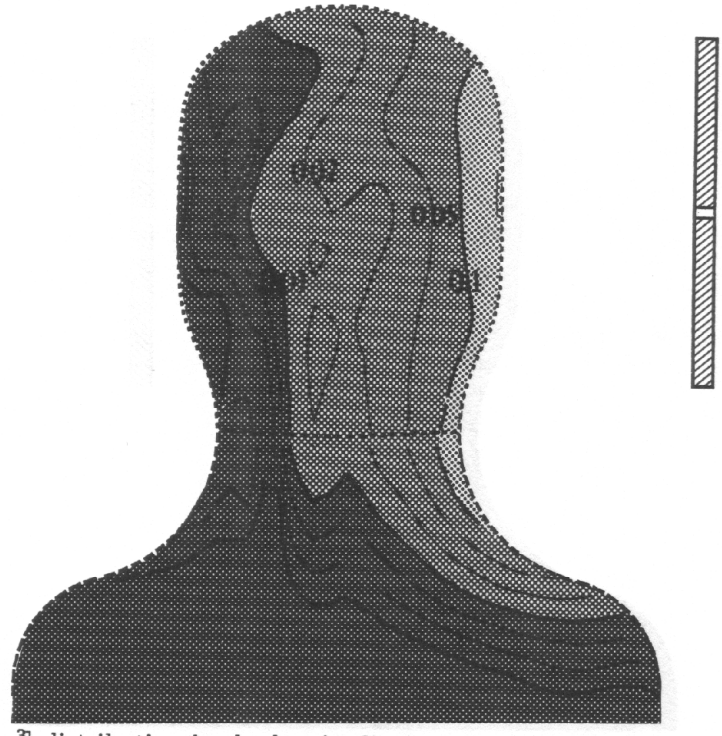

Figure 7: SAR [mW/cm^3] distribution in the longitudinal section. Simulation of the body mounted UHF antenna (f = 750 MHz) at a distance of 10 cm from the surface of the head. The parameters of the simulation are: $I_{fp} = 141$ mA; head: $\varepsilon_r = 45$, $\sigma = 0.75$ mho/m (brain tissue); body: $\varepsilon_r = 55$, $\sigma = 1.4$ mho/m (muscle tissue).

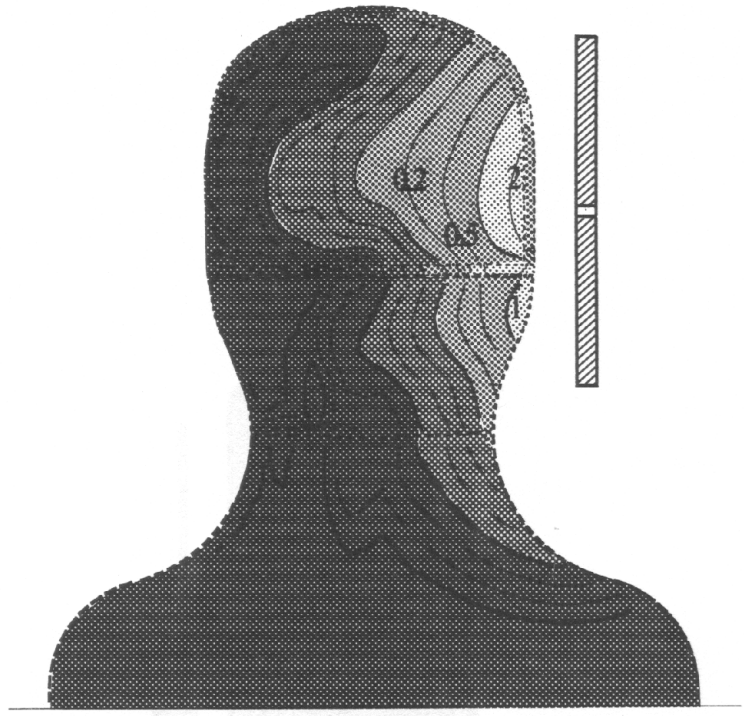

Figure 8: SAR [mW/cm^3] distribution in the longitudinal section of the refined model including skull bones. Simulation of the body mounted UHF antenna (f = 750 MHz) at a distance of 2.5 cm from the surface of the head. The parameters of the simulation are: $I_{fp} = 141$ mA; brain: $\varepsilon_r = 45$, $\sigma = 0.75$ mho/m (brain tissue); skull: $\varepsilon_r = 5$, $\sigma = 0.15$ mho/m (correspond to bone tissue); neck and rest of the body: $\varepsilon_r = 55$, $\sigma = 1.4$ mho/m (muscle tissue).

distribution for different human models and transmitter types. As this does not greatly change with the distance d between the longitudinal axis of the antenna and the body surface, only a few representative examples are shown.

The solutions verify the expected relation [Kuster and Balzano, 1992] between the spatial distribution of the absorbed power and the spatial magnetic field distribution or the current distribution on the antenna surface, respectively. When comparing the solution of the refined model (Figure 8) with that of the homogeneous one (Figure 5), it is, at first glance, surprising that higher SAR values are found in the lower conducting skull base than in the nearby brain or muscle tissue. This is explained by the fact that the main component of the induced electric field is normal to the surface of the brain, bone and muscle tissue, which have strongly different dielectric properties. The peak local SAR values (2.2 mW/cm^3, and 15 mW/10 cm^3, respectively) are lower than that of the homogeneous head (Figure 5) not because of any screening effect of the skull but because of the greater distance (d + thickness of the skull) between the more conductive and absorbent brain tissue and the antenna axis. Figure 8 and Figure 10 in particular clearly show that inhomogeneity modifies the absorption distribution only locally and does not lead to significant changes. From this, it follows that models of higher complexity should only be used to study specific effects in detail, e.g., the absorption in the vitreous body of the eye or in its crystalline lens. Otherwise the validation of the solution becomes extremely tedious or even impossible.

The calculation of the numerical value of the peak local SAR averaged over a given volume is carried out as follows. First the point of highest absorption is determined by a scanning procedure. The averaged SAR values around this point are then computed in cubes of volume at 1 cm^3, 10 cm^3 and 100 cm^3 by numerical integrations. Highest resolution is given because the fields inside the

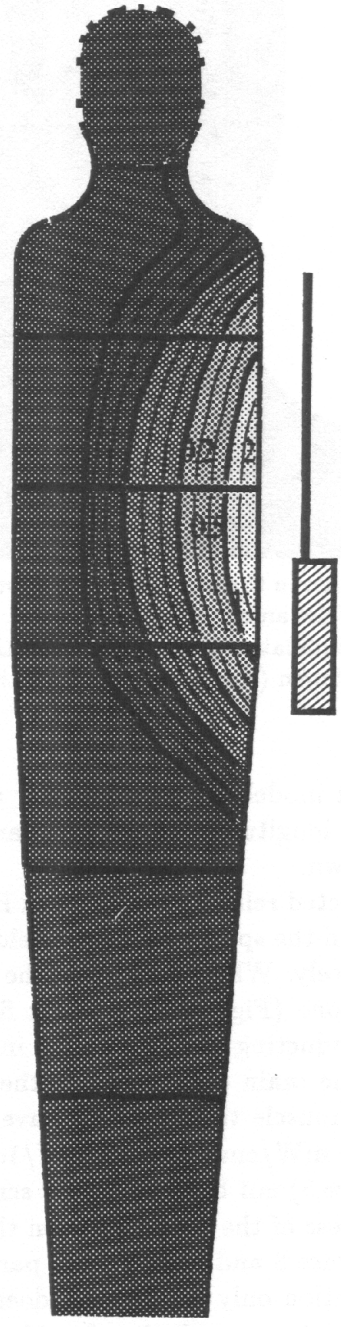

Figure 9: SAR [mW/cm^3] distribution in the longitudinal section. Simulation of VHF version of the newer devices (f = 200 MHz) with a monopole antenna mounted on the device at a distance of 5 cm from the surface of the body. The parameters of the simulation are: $I_{fp} = 447$ mA; head: $\varepsilon_r = 70$, $\sigma = 0.45$ mho/m (which correspond to brain tissue); body: $\varepsilon_r = 75$, $\sigma = 0.95$ mho/m (muscle tissue).

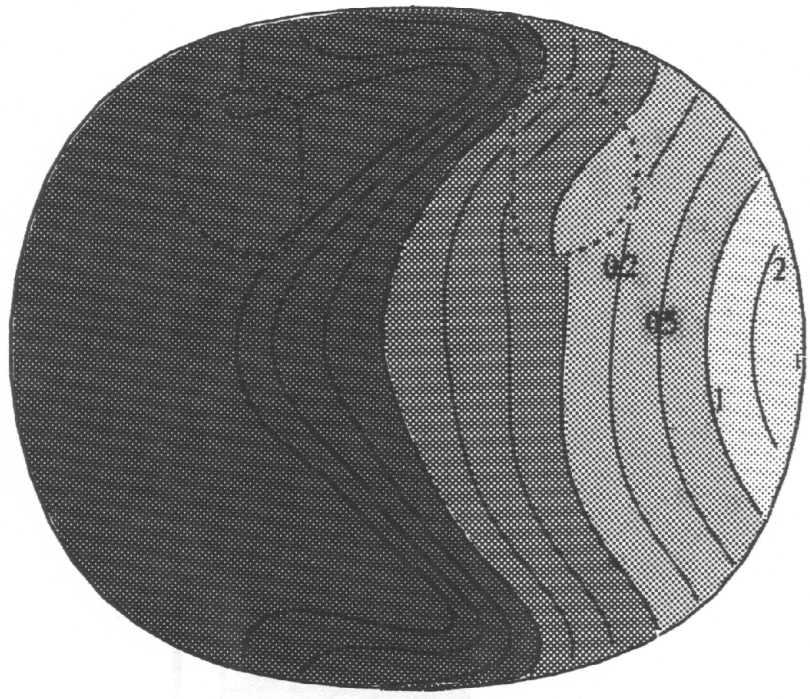

Figure 10: SAR [mW/cm^3] distribution in the cross section at the level of the antenna feedpoint. Simulation of VHF version of the newer devices (f = 200 MHz) with a monopole antenna mounted on the device at a distance of 5 cm from the surface of the body. The parameters of the simulation are: $I_{fp} = 447$ mA; head: $\varepsilon_r = 120$, $\sigma = 0.4$ mho/m (which correspond to brain tissue); body: $\varepsilon_r = 100$, $\sigma = 0.8$ mho/m (muscle tissue); kidneys: $\varepsilon_r = 180$, $\sigma = 1.0$ mho/m (kidney tissue).

tissue are Maxwell fields, i.e., the volumes do not need to be discretized into a large number of cells in which the fields are approximated by linear functions.

The values in Table 1 and 2 are calculated by a series of simulations varying the distance d with the given model (Figure 2). For the computation of the local SARs for Table 3 and 4, an even more simplified model can be applied. In this case, the solution validation process, which is performed according to [Kuster, 1993], shows that the spatial local peak SAR values varies only within 1dB if a cylindrical model (length = 175 cm, diameter = 12 cm) and a symmetrical dipole are used instead of the initial models (Figures 9 and 10). This significantly reduced the required computer time without altering the reliability of the tables. It is important to note that the degree of E-field coupling depends on the resonance properties of the body in the case of greater distances. Therefore, the absorption strongly depends on the body, especially for larger distances. In order to obtain worst case estimates, the length of the cylinder used is close to resonance.

Only the values for the shoulder-mounted VHF monopole antenna must be estimated (Table 3). This is due to the fact that, although the radiating monopole is a few cm from the body surface, the electrical counterpoise combined with feeding line ($\lambda/4$ choke) is practically attached to the shoulder. A simulation of this situation would require a completely different modeling. In addition, the factors which govern the direct coupling to the body would have to be determined. All this would be extremely time consuming and is not performed because reliable estimates can be obtained with the given models. The values are extrapolated using the results when d =1.25 cm and d =0.65 cm and when the antenna is actually inside the muscle tissue. The exact SAR distribution cannot be given. However, it is obvious that the maximum values lie in the shoulder region.

If the values of Tables 1 to 4 are compared with the values obtained by the approximation

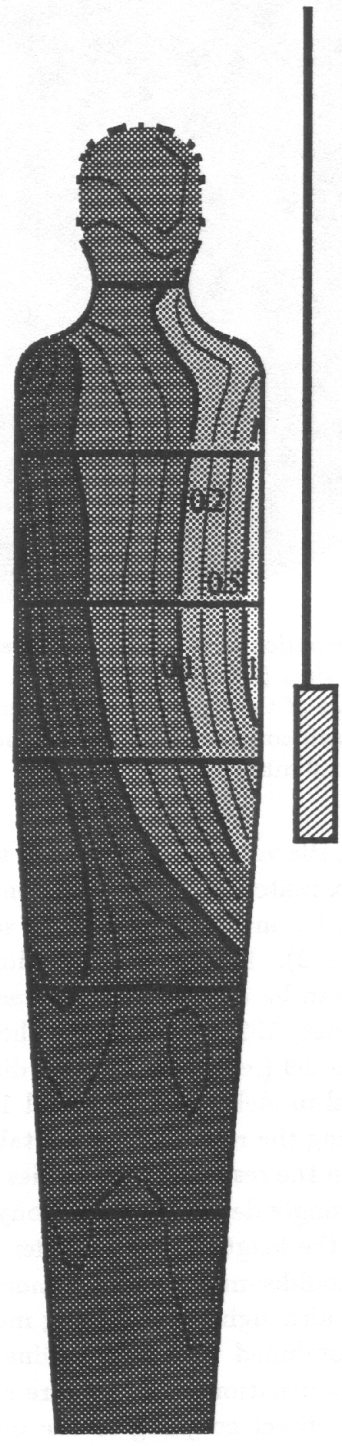

Figure 11: SAR [mW/cm^3] distribution in the longitudinal section. Simulation of an older devices (f = 80 MHz) with a monopole antenna mounted on the device at 5 cm distance from the body surface. The parameters of the simulation are: $I_{fp} = 447$ mA; head: $\varepsilon_r = 120$, $\sigma = 0.4$ mho/m (which correspond to brain tissue); body: $\varepsilon_r = 100$, $\sigma = 0.8$ mho/m (muscle tissue).

f [MHz]	d [cm]	SAR_p [mW/cm^3]	SAR_{av1cm^3} [mW/cm^3]	SAR_{av10cm^3} [mW/cm^3]	$SAR_{av100cm^3}$ [mW/cm^3]
750	2.5	6.0	4.0	2.5	1.0
750	10.0	0.36	0.26	0.17	0.09
550	2.5	4.3	2.9	1.9	0.90
550	10.0	0.27	0.20	0.14	0.08

Table 1: Spatial local peak SAR averaged over different volumes with the body mounted UHF antenna (shoulder-belt) ($I_{fp} = 141$ mA). Both body and head are simulated with the electrical properties of muscle tissue. These values can be not only considered as a worst case for the head, but also as a good approximation for the case if the antenna is mounted on the device enclosure. This is because the different curvature between head and body do not significantly modify the peak SAR values for this wavelength.

f [MHz]	d [cm]	SAR_p [mW/cm^3]	SAR_{av1cm^3} [mW/cm^3]	SAR_{av10cm^3} [mW/cm^3]	$SAR_{av100cm^3}$ [mW/cm^3]
750	2.5	4.1	3.0	2.1	1.1
750	5.0	1.1	0.85	0.64	0.37
750	10.0	0.25	0.20	0.15	0.10
550	2.5	2.9	2.2	1.6	0.85
550	10.0	0.19	0.15	0.12	0.09

Table 2: Spatial local peak SAR values averaged over different volumes for the UHF transmitters with the body mounted antenna ($I_{fp} = 141$ mA). Both body and head are simulated with the electrical properties of muscle and brain tissue, respectively.

formula (assuming an attenuation given by the skin effect), then the approximation values are lower than the computed ones for the VHF devices. The difference increases with larger distances d due to the resonance coupling mentioned above.

3.5 Assessment

Safety distances can be assessed using the summarized solutions above and the approximation given in [Kuster and Balzano, 1992]. The new draft of the DIN VDE norm [DIN VDE 0848 Part 2, 1991] considers 10 W/kg (Environment 1) as the basic limiting value for spatial local peak SAR values, whereby the average must be taken for each 10 g of muscle tissue and at each 6 minute intervals. For the extremities, such as the hand, wrist, foot and ankle, 20 W/kg are tolerated. Within Environment 2, the values are reduced by a factor of 5, i.e., 2 W/kg and 4 W/kg, respectively. The

f [MHz]	d [cm]	SAR_p [mW/cm^3]	SAR_{av1cm^3} [mW/cm^3]	SAR_{av10cm^3} [mW/cm^3]	$SAR_{av100cm^3}$ [mW/cm^3]
200	body mounted	7*	5*	3*	1.5*
200	2.5	1.5	1.2	0.95	0.56
200	5.0	0.70	0.58	0.47	0.30
200	10.0	0.27	0.23	0.19	0.13
200	20.0	0.08	0.07	0.06	0.04

Table 3: Spatial local peak SAR values averaged over different volumes for the VHF version of the newer devices with the monopole antenna mounted on the device enclosure ($I_{fp} = 141$ mA). The values for the body mounted antenna (shoulder belt) were approximated from different simulations (*).

f [MHz]	d [cm]	SAR_p [mW/cm^3]	SAR_{av1cm^3} [mW/cm^3]	SAR_{av10cm^3} [mW/cm^3]	$SAR_{av100cm^3}$ [mW/cm^3]
80	2.5	0.41	0.35	0.29	0.19
80	5.0	0.23	0.20	0.17	0.12
80	10.0	0.11	0.10	0.09	0.07
80	20.0	0.05	0.05	0.04	0.03

Table 4: Spatial local peak SAR values averaged over different volumes for the older VHF transmitters with the monopole antenna mounted on the device enclosure ($I_{fp} = 141$ mA).

major differences in the safety limits defined by IEEE [IEEE, 1992] and the IRPA [IRPA, 1988] are in the tissue mass upon which the average is based (1 g and 100 g, respectively). As discussions on the most appropriate tissue mass have not yet come to an end, the safety distances for the three volumes 1 cm^3, 10 cm^3, and 100 cm^3 are calculated.

These distances are summarized in Tables 5 and 6 for both Environments 1 and 2 (10 W/kg and 2 W/kg). By applying the DIN VDE norm, the limit of Environment 1 must be applied for the reportage transmitter since the exposure is brief (less than 6 hours a day). According to this, a distance of only 2.5 cm for all devices would be sufficient, assuming a 50 Ω feedpoint impedance. This distance must be increased to 3.5 cm if the limits are based on 1 cm^3. If we require that the values for 2 W/kg (Environment 2) must be respected, the necessary distance becomes 10 cm. For the body-mounted (shoulder belt) VHF antenna, a safety distance cannot be given because the safety limits are already violated independently of the distance to the head by the strong direct coupling to the shoulder.

Finally, possible deviations from the values given in this report to those for real devices and human beings must be discussed.

The used dipole model is highly suited to simulate the UHF transmitting antenna. For this reason, it is believed that no coarse violation of the limits should occur for distances greater than the safety distances given here.

The situation is less defined for the VHF transmitter. In these cases, because the enclosure represents the electrical counterpoise for the monopole antenna, the impedance, as well as the HF current distribution on the enclosure in function of the distance, is not accurately known. However, reliable information would be important because the induced power is proportional to the square of the magnetic field at the body surface [Kuster and Balzano, 1992]. These uncertainties can be taken into account by a safetyfactor of 2, i.e., by 1.4 times larger distances, making the limits now highly reliable. The only exception is the VHF antenna, as it must be assumed, that the limits are violated in the shoulder region in any case.

In conclusion, the investigated transmitters are in compliance with the limits for Environment 2 of DIN VDE 0848 Part 2, if a minimum distance of 4 cm from the body is respected. Only the use of the body-mounted VHF monopole antenna cannot be recommended.

4 Conclusion

The MMP codes are applicable to static or time-harmonic electromagnetic boundary value and eigenvalue problems with piecewise linear and homogeneous domains. Consequently, inhomogeneities can only be simulated by several homogeneous subdomains for each of which appropriated basis functions must be set up. At first sight, this appears to be a serious drawback to this approach as compared to FDTD. However, in most cases the inhomogeneities of biological bodies modify the

f [MHz]	P [W]	ant-mount method	d($1cm^3$ av) [cm]	d($10cm^3$ av) [cm]	d($100cm^3$ av) [cm]
550-750	1	B,D	1.5	1.5	1
550-750	3	B,D	3	2	1.5
200	10	D	3.5	2.5	2
80	10	D	1.5	1.5	1

Table 5: Safety distances up to those of the limits for 10 W/kg is reached, which are only valid for the methods of antenna mounting (ant-mount) given in the Table (B = body mounted: the antenna is mounted on the shoulder belt; D = mounted on the device enclosure). These values assume a feedpoint impedance of 50 Ω.

f [MHz]	P [W]	ant-mount method	d($1cm^3$ av) [cm]	d($10cm^3$ av) [cm]	d($100cm^3$ av) [cm]
550-750	1	B,D	4	3.5	2
550-750	3	B,D	7	6	3.5
200	10	D	11	10	7
80	10	D	4	3.5	3

Table 6: Safety distances according to Table 5 for the safety limits of 2 W/kg.

field distribution only locally beyond the uncertainties of the models. In these cases, the modeling of only the local inhomogeneities or disturbances, which are of interest, might be preferable because the simulations are more easily controlled and validated.

On the other hand, MMP has important advantages: 1) the modeling effort is reduced by one dimension because the basis functions are analytical solutions of the Maxwell equations and only the boundary conditions are numerically approximated, i.e., only the boundary must be discretized (also in the case of lossy materials). This allows fast and convenient creation and modification of the geometry with a graphical interface. 2) The modeling of wire objects is done as easily as with MoM codes such as NEC. 3) Multipoles are excellent expansion functions to match local disturbances, i.e., locations where high gradient fields occur. 4) The validation effort is also reduced by one dimension due to the same reasons as the modeling. This empowers reliable validation of the quantitative results on a numerical basis. 5) Any fields and integrals are easily computed because the solution corresponds to a Maxwell field in any point.

Because of the method's flexibility and efficiency in modeling and solving geometrically simple problems, the MMP codes are successfully employed in EMF education. However, they are also best suited for a wide range of scientific and commercial applications, in particular, for biomedical computations.

5 Acknowledgment

The author gratefully acknowledge the help of Mr. M. Dahme from the IRT. The safety study was supported by a grant from the Research and Development Center of the Public Broadcasting Organization (IRT) in Germany.

References

L. Bomholt, *MMP-3D — A Computer Code for Electromagnetic Scattering Based on the GMT.* PhD thesis, Diss. ETH No. 9225, 1990.

J.-Y. Chen and O. P. Gandhi, "Electromagnetic deposition in an anatomically based model of man for leakage fields of a parallel-plate dielectric heater," *IEEE Transactions on Microwave Theory and Techniques*, vol. 37, pp. 174–180, Jan. 1989.

DIN VDE 0848 Teil 2 (Entwurf), *Sicherheit in elektromagnetischen Feldern - Schutz von Personen im Frequenzbereich von 30 kHz bis 300 GHz.* VDE-Verlag GMBH, Berlin 12: Deutsche Norm, Oct. 1991.

W. M. Gentleman, "Error analysis of QR decompositions by Givens transformations," *Linear Algebra and its Applications*, vol. 10, pp. 189–197, 1975.

G. H. Golub and C. F. Van Loan, *Matrix Computations.* Johns Hopkins University Press, 2nd ed., 1989.

Ch. Hafner, *The Generalized Multipole Technique for Computational Electromagnetics.* Artech House Books, 1990.

Ch. Hafner, *2D-MMP: Two Dimensional Multiple Multipole Analysis Software and User's Manual.* Artech House Books, 1990.

Ch. Hafner and N. Kuster, "Computations of electromagnetic fields by the MMP method (GMT)," *Radio Science*, vol. 26, pp. 291–297, Feb. 1991.

IEEE C95.1-1991, *IEEE Standard for Safety Levels with Respect to Human Exposure to Radio Frequency Electromagnetic Fields, 3 kHz to 300 GHz.* Inc., New York, NY 10017: The Institute of Electrical and Electronics Engineers, 1992.

International non-ionizing radiation committee of the international radiation protection association, "Guidelines on limits of exposure to radiofrequency electromagnetic fields in the frequency range from 100kHz to 300GHz," *Health Physics*, vol. 54, pp. 115–123, Jan. 1988.

M. Iskander, S. C. Olson, and J. McCalmont, "Near field absorption characteristics of biological models in the resonance frequency range," *IEEE Transactions on Microwave Theory and Techniques*, vol. 35, pp. 776–780, Aug. 1987.

N. Kuster and R. Ballisti, "MMP-method simulation of antennae with scattering objects in the closer nearfield," *IEEE Transactions on Magnetics*, vol. 25, pp. 2881–2883, July 1989.

N. Kuster and Q. Balzano, "Energy absorption mechanism by biological bodies in the near field of dipole antennas above 300 MHz," *IEEE Transaction on Vehicular Technology*, vol. 41, pp. 17–23, Feb. 1992.

N. Kuster, "Use of the multiple multipole technique for simulating EM problems involving biological bodies," submitted to Transactions on Biomedical Engineering.

N. Kuster and L. Bomholt, "A block iterative technique to expand MMP's applicability to EM problems of higher complexity," submitted to Transactions on Antenna and Propagation.

P. Leuchtmann, "New expansion functions for long structures in the MMP-code," in *7th Annual Review of Progress in Applied Computational Electromagnetics (ACES), Conference Proceedings*, (Monterey), Mar. 1991.

A. Ludwig, "A new technique for numerical electromagnetics," *IEEE AP-S Newsletter*, vol. 31, pp. 40–41, Feb. 1989.

P. Regli, Ch. Hafner, and N. Kuster, "Graphic output routines of the MMP-program package on PC's and SUN workstations," in *5th Annual Review of Progress in Applied Computational Electromagnetics (ACES), Conference Proceedings*, (Monterey), Mar. 1989.

M. A. Stuchly, R. J. Spiegel, S. S. Stuchly, and A. Kraszewski, "Exposure of man in the near-field of a resonant dipole: Comparision between theory and measurements," *IEEE Transactions on Microwave Theory and Techniques*, vol. 34, pp. 26–31, Jan. 1986.